Generalized liquid drop model and fission, fusion, alpha and cluster radioactivity and superheavy nuclei

Guy Royer

GENERALIZED LIQUID DROP MODEL AND FISSION, FUSION, ALPHA AND CLUSTER RADIOACTIVITY AND SUPERHEAVY NUCLEI

G. Royer

Laboratoire Subatech, UMR: IN2P3/CNRS-Université-Ecole des Mines, Nantes, France

A particular version of the liquid drop model taking into account both the mass and charge asymmetries, the proximity energy, the rotational energy, the shell and pairing energies and the temperature has been developed to describe smoothly the transition between one and two-body shapes in entrance and exit channels of nuclear reactions. In the quasi-molecular shape valley where the proximity energy is optimized, the calculated l-dependent fusion and fission barriers, alpha and cluster radioactivity half-lives as well as actinide half-lives are in good agreement with the available experimental data. In this particular deformation path, double-humped potential barriers begin to appear even macroscopically for heavy nuclear systems due to the influence of the proximity forces and, consequently, quasi-molecular isomeric states can survive in the second minimum of the potential barriers in a large angular momentum range.

1. Introduction

The fission shapes were firstly investigated long time ago by minimizing the sum of the Coulomb and surface energies using mainly a development of the radius in Legendre polynomials. This leads to fission valley through very elongated shapes with shallow necks and difficulties to precise the position of the scission point where the rupture of the bridge of matter between the nascent fragments occurs.

More recently, the fusion studies have shown that the picture of the pure Coulomb barrier is not sufficient to obtain correct fusion cross sections. It is necessary to take into account the effects of the nuclear forces in the gap between the incoming close nuclei or in the crevice where the neck is formed in adding a proximity energy term.

So we have defined a Generalized Liquid Drop Model (GLDM) including this proximity energy and a quasi-molecular shape sequence to describe firstly the fusion process and, later on, to study whether, in this deformation valley which optimizes the proximity energy, the fission data may also be reproduced. Calculations show that degeneracy exists effectively between the energy of elongated shapes found by the liquid drop model without proximity energy and the energy of compact and necked shapes which is lowered by the introduction of the nuclear proximity effects. The agreement with the fusion and fission data has finally led to the study of the alpha and cluster radioactivity and the entrance and exit channels of superheavy nuclei.

2. Generalized Liquid Drop Model

For an arbitrary deformed nucleus, the macroscopic total energy is the sum of the Rotational Liquid-Drop Model energy and the nuclear proximity energy [1]. Constant density and volume conservation are assumed.

$$E_{RLDM} = E_V + E_S + E_C + E_{Rot} . \quad (1)$$

For one-body shapes, the volume E_V, surface E_S and Coulomb E_C energies are given by :

$$E_V = -a_v(1-k_v I^2)A , \quad (2)$$

$$E_S = a_s(1-k_s I^2)A^{2/3}(S/4\pi R_0^2) , \quad (3)$$

$$E_C = 0.6e^2(Z^2/R_0)\cdot 0.5\int (V(\theta)/V_0)(R(\theta)/R_0)^3 \sin\theta d\theta \quad (4)$$

where A, Z and I = (N - Z)/A are the mass, charge and relative neutron excess of the compound nucleus. $V(\theta)$ is the electrostatic potential at the surface of the shape and V_0 the surface potential of the sphere. The volume and surface coefficients a_v, a_s and the effective sharp radius R_0 are defined as :

$$a_v(T) = 15.494(1+0.00337T^2) \text{ MeV} , \quad (5)$$

$$a_s(T) = 17.9439\ (1+1.5T/17)(1-T/17)^{3/2} \text{ MeV} , \quad (6)$$

$$R_0(T) = (1.28A^{1/3} - 0.76 + 0.8A^{-1/3})(1+0.0007\ T^2) \text{ fm} . \quad (7)$$

This later formula leads to an increase of the ratio $r_0 = R_0/A^{1/3}$ with the mass; for example, $r_0 =$ 1.11 fm for ^{20}Ne and $r_0 =$ 1.18 fm for ^{240}Pu. For comparison, the potential defined by Krappe, Nix and Sierk [2] assumes $a_s =$ 21.7 MeV

and $r_0 =$ 1.18 fm while the recent version of the Thomas-Fermi model [3] supposes $a_s =$ 18.63 MeV and $r_0 =$ 1.14 fm. The surface and volume asymmetry coefficients take on the values:

$$k_s = 2.6 \qquad \text{and} \qquad k_v = 1.8 \,. \tag{8}$$

Discussions on the different possible coefficients of the macro-microscopic mass formulas can be found in Ref. [4].

When the two fragments (or colliding nuclei) are separated:

$$E_V = -a_v \left[(1 - k_v I_1^2) A_1 + (1 - k_v I_2^2) A_2 \right], \tag{9}$$

$$E_S = a_s \left[(1 - k_s I_1^2) A_1^{2/3} + (1 - k_s I_2^2) A_2^{2/3} \right], \tag{10}$$

$$E_c = \frac{3}{5} e^2 Z_1^2 / R_1 + \frac{3}{5} e^2 Z_2^2 / R_2 + e^2 Z_1 Z_2 / r \,, \tag{11}$$

where A_i, Z_i, R_i and I_i are the masses, charges, radii and relative neutron excesses of the fragments and r the distance between the mass centers. The discontinuity of a few MeV which appears at the contact point when Z_1/A_1 and Z_2/A_2 are very different has been removed linearly from the contact point to the sphere since it is due to the progressive rearrangement of the nuclear matter.

The surface energy E_S takes only into account the effects of the surface tension forces in an half space and does not include the contribution due to the attractive nuclear forces between the surfaces in regard in the neck or the gap between nascent fragments or incoming nuclei. The nuclear proximity energy term E_N takes into account these additional surface effects when crevices appear in the deformation path [1].

$$E_N = 2\gamma \int_{h_{\min}}^{h_{\max}} \varphi(D/b) 2\pi h dh \,. \tag{12}$$

h is the ring radius in the plane perpendicular to the fission axis and D the distance between the infinitesimal surfaces in regard. b is the surface width fixed at 0.99 fm. ϕ is the proximity function. The surface parameter γ is given by a geometric mean between the surface parameters of the two fragments:

$$\gamma = 0.9517 \sqrt{(1 - k_s I_1^2)(1 - k_s I_2^2)} \ \text{MeV.fm}^{-2}. \tag{13}$$

In this GLDM the surface diffuseness is not considered and the proximity energy vanishes when there is no neck.

The rotational energy has been determined within the rigid body ansatz. Indeed, it has been shown that corrective terms arising from the orbital motion and the spin degrees of freedom roughly cancel each other, particularly at large deformations.

$$E_{Rot} = \frac{\hbar^2 l(l+1)}{2 I_\perp} \,. \tag{14}$$

Microscopic corrections have been added to this macroscopic energy. The shell corrections have been introduced [5] as defined in the Droplet Model with an attenuation factor given by

$$E_{Shell} = E_{Shell}^{sphere} (1 - 2.6\alpha^2) \exp(-\alpha^2), \quad \text{where} \quad \alpha^2 = (\delta R)^2 / a^2 \,. \tag{15}$$

The distortion αa is the root mean square of the deviation of the surface from a sphere, a quantity which incorporates all types of deformation indiscriminately. Using this approach, shell corrections only play a role near the ground state of the compound nucleus and not at the saddle-point (where they are expected to be of the order of 1 MeV or smaller). The pairing energy of the recent Thomas - Fermi model [3] has been selected.

A two parameter shape sequence has been defined [1] to describe the continuous transition from one spherical nucleus to two tangent spherical nuclei (see Fig. 1).

$$R(\theta)^2 = \begin{cases} a^2 \sin^2\theta + c_1^2 \cos^2\theta & (0 \le \theta \le \pi/2) \\ a^2 \sin^2\theta + c_2^2 \cos^2\theta & (\pi/2 \le \theta \le \pi) \end{cases}. \tag{16}$$

c_1 and c_2 are the two radial elongations and a the neck radius. Assuming volume conservation, the two parameters $s_1 = a/c_1$ and $s_2 = a/c_2$ completely define the shape. When s_1 decreases from 1 to 0 the shape evolves from one sphere

to two touching spheres with the formation of a deep neck while keeping almost spherical ends. Using the axial symmetry, analytical expressions have been obtained for the various shape-dependent functions: volume, surface, moment of inertia, distance between the mass centres of each fragment and quadrupole moment.

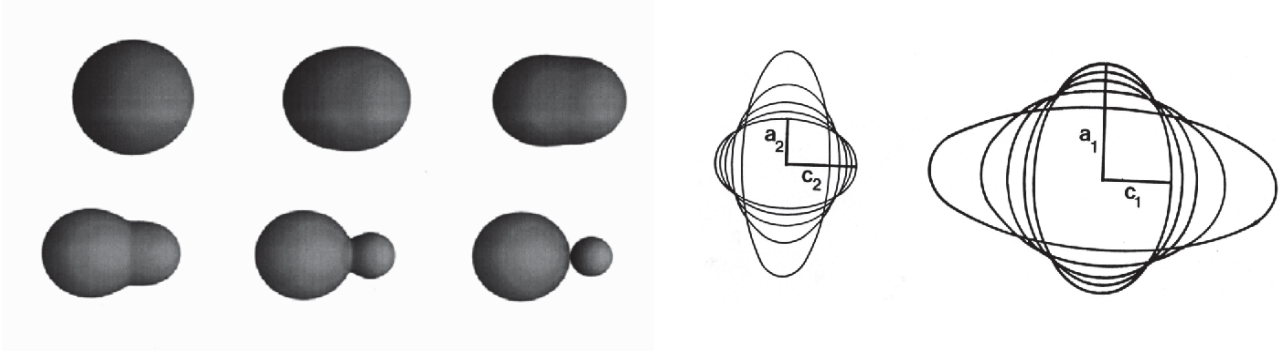

Fig. 1. Shape sequences describing the one-body shape evolution and the two coaxial ellipsoid configurations. The fission axis is the common axis of revolution.

The two coaxial ellipsoid configurations or simply the two-sphere approximation have been used to describe the two-body shapes.

3. Fusion

The main characteristics which govern the fusion process are the barrier height and the position of its maximum. The GLDM allows a correct reproduction of these empirical data deduced from the fusion cross sections ([1, 6] and Table 1). Double-humped fusion barriers appear when $Z_1Z_2 \geq 1800 \pm 100$. The inner barrier is the highest for $Z_1Z_2 \geq 2300 \pm 100$. The existence and the shape of the external minimum due to the proximity energy is at the origin of the development of fusion-fission and fast fission phenomena. Using a simple dynamic model it has been shown that a dynamic fusion barrier appears for very heavy systems ($Z_1Z_2 \geq 2100 \pm 100$), significantly higher than the static one and in close agreement with the experimental data. This dynamic barrier is mostly governed by the entrance channel. The possibility of forming superheavy elements in almost symmetric reactions is strongly hindered by this double-humped dynamic barrier.

Table 1. **Comparison between the experimental fusion barrier heights E_{0f} and positions R_{0f} and the theoretical predictions of the Krappe, Nix and Sierk potential and of the GLDM**

Reaction	Z_1Z_2	$E_{of,Exp}$ (MeV)	$R_{of,Exp}$ (fm)	$E_{of,Th}$ (KNS)	$R_{of,Th}$ (KNS)	$E_{of,Th}$ (GLDM)	$R_{of,Th}$ (GLDM)
$^{9}Be + ^{10}B$	20	3.4	7.65	3.36	7.77	3.36	7.79
$^{4}He + ^{44}Ca$	40	6.37	8.25	6.19	8.5	6.2	8.51
$^{16}O + ^{26}Mg$	96	15.24	8.29	14.69	8.59	14.82	8.56
$^{4}He + ^{209}Bi$	166	20.52	10.88	20.58	10.77	20.46	10.93
$^{34}S + ^{26}Mg$	192	27.11	9.5	27.63	9.16	27.84	9.17
$^{16}O + ^{110}Pd$	368	46.2	-	48.0	10.17	48.05	10.26
$^{40}Ar + ^{58}Ni$	504	65.3	-	66.74	9.99	66.76	10.07
$^{40}Ca + ^{58}Ni$	560	73.36	10.2	73.89	10.02	74.72	9.98
$^{35}Cl + ^{90}Zr$	680	84.87	10.74	86.73	10.39	86.5	10.51
$^{86}Kr + ^{58}Ni$	1008	120.8	-	123.55	10.82	122.77	10.95
$^{40}Ar + ^{144}Sm$	1116	130.2	-	132.01	11.23	130.96	11.37
$^{40}Ar + ^{174}Yb$	1260	139	-	144.83	11.58	143.39	11.76
$^{40}Ar + ^{177}Hf$	1296	145	-	148.67	11.6	147.19	11.76
$^{81}Br + ^{90}Zr$	1400	156	-	164.79	11.26	163.29	11.42
$^{81}Br + ^{104}Ru$	1540	174	-	178.01	11.48	176.18	11.61

For light systems and energy around the Coulomb barrier the static approach is sufficient to reproduce the fusion cross sections. At higher energies the increase of the fusion cross section with incident energy is limited by a strong dissipation occurring around the contact point. With increasing mass the slope of the fusion cross sections is better reproduced if the angular momentum dissipation rule varies from the sticking limit for medium systems to the sliding limit for very heavy systems [1].

4. Fission

The different contributions to the deformation energy are given for the ^{160}Dy nucleus in Fig. 2. The E_s and E_n curves change drastically at the contact point since the surface is constant after the separation and the nuclear attraction is greatest at the contact point. Nevertheless, the total energy varies gently even around the contact point. Moreover the barrier height corresponds to the fission barrier height [7]. In the right part of Fig. 2 the deformation energies of the ^{234}U nucleus corresponding to different shape sequences with and without proximity energy contribution are compared. The potential energy calculated using quasi-molecular shapes without taking into account the proximity energy is very energetically unfavourable . On the contrary, when the proximity energy is included for the same shape sequence, the barrier height may be compared with the barrier height of the potential energy for usual elongated and little or not creviced shapes [5]. Furthermore, a double-humped barrier appears even macroscopically for the compact and necked shapes. This shows clearly that the comparison between the two shape sequences must be re-examined when the additional proximity energy term is introduced. The two spheroid shapes would be also highly competitive with regard to the usual elongated shapes if the proximity energy was included since this term is large when there is a deep gap and negligible for elongated shapes with a shallow neck.

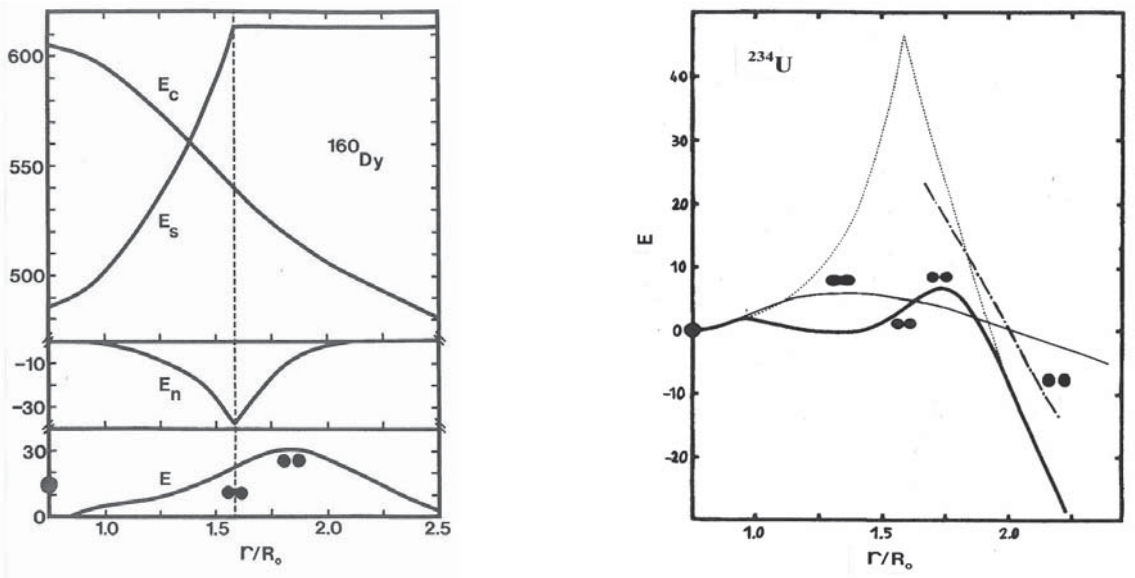

Fig. 2. On the *left part*, contribution of the Coulomb, surface and nuclear proximity energies to the total deformation energy E of the ^{160}Dy. The dotted line indicates the contact point between spherical fragments. On the *right part*, the thick full curve and the dotted curve are respectively the potential energies using our quasi-molecular shape sequence with and without proximity energy. The thin full curve is the energy of elongated shapes while the chain curve gives the energy of two separated oblate spheroids with no proximity contribution.

The usual picture of the Businaro - Gallone point assuming that, macroscopically, asymmetric fission is favoured for light systems and symmetric fission for heavy nuclei is also observed in the quasi-molecular shape path (see Fig. 3). More generally, it has been proved that the deformation barrier heights in this valley correspond precisely to the experimental fission barrier heights [5].

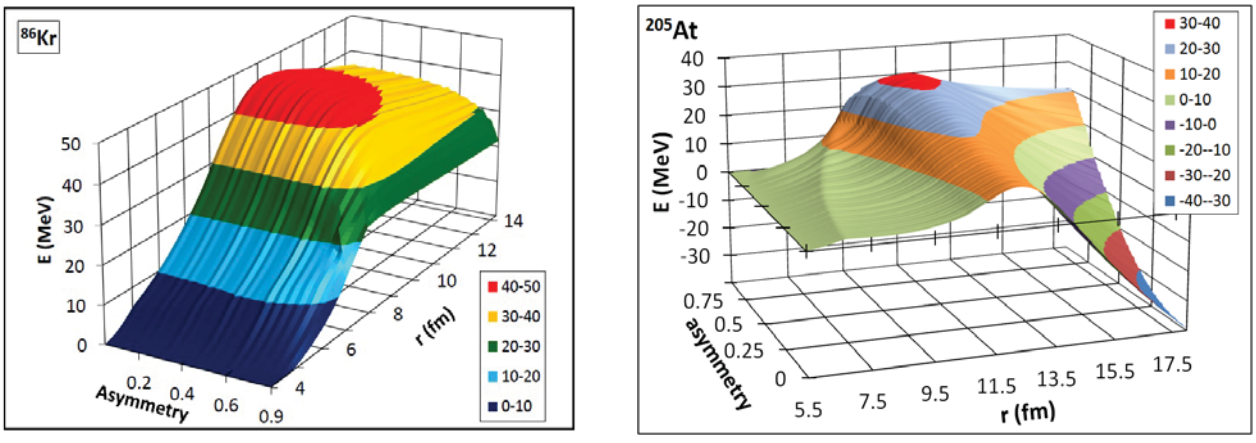

Fig. 3. Macroscopic fission barriers as functions of the decay asymmetry $(A_1 - A_2)/(A_1 + A_2)$ and the distance between the mass centers r for the two ^{86}Kr and ^{205}At nuclei.

In the *left part* of Fig. 4 the mass evolution of the barrier profile is displayed. With increasing mass appear macroscopically a plateau and a second external relative minimum and internal peak due to the proximity energy and then the possibility of isomeric states. On the right, for ^{152}Dy but this is a general behaviour, it is shown that the rotation of a quasi-molecular shape creates also strongly deformed rotating isomeric states [6, 8].

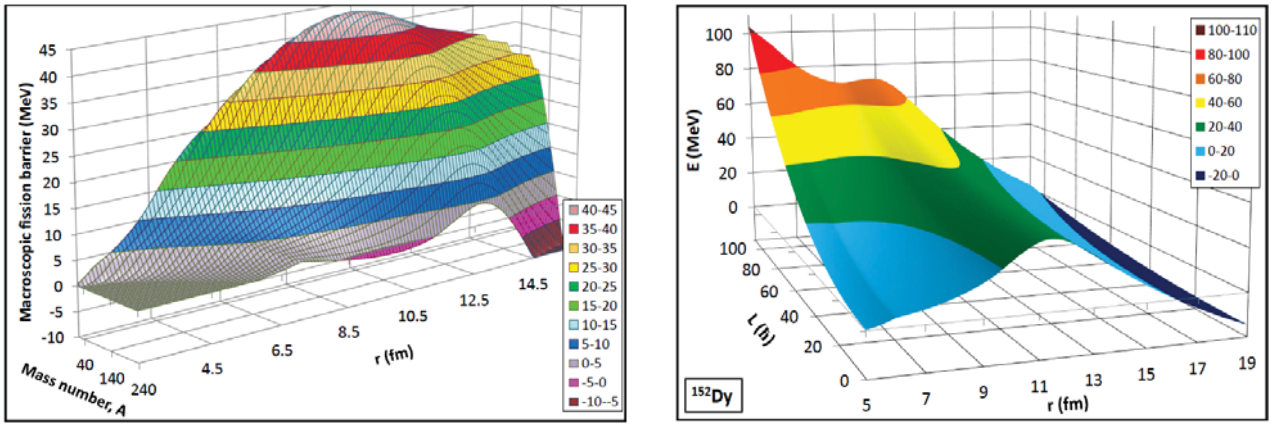

Fig. 4. Symmetric fission barrier as functions of the mass in the β-stability valley (on the *left*) and symmetric fission barrier of the ^{152}Dy nucleus versus the angular momentum (on the *right*).

In Fig. 5 the shell and pairing energies have been introduced as well as the ellipsoidal deformations to calculate the fission barriers of ^{240}Pu, as an example. Multiple-humped potential barriers appear. The second maximum corresponds to the transition from compact and creviced one-body shapes to two touching ellipsoids. Shallow third minimum and peak appear in specific asymmetric exit channels where one fragment is close to a double magic quasi-spherical nucleus while the other one evolves from oblate to prolate shapes. The heights of the potential barriers agree with the experimental data and the calculated half-lives follow the trend of the experimental values. The complete separation of the fragments corresponds to a sudden shape change and to the vanishing of the proximity energy. It occurs on an energy plateau corresponding to the fragment kinetic energy plus excitation energy.

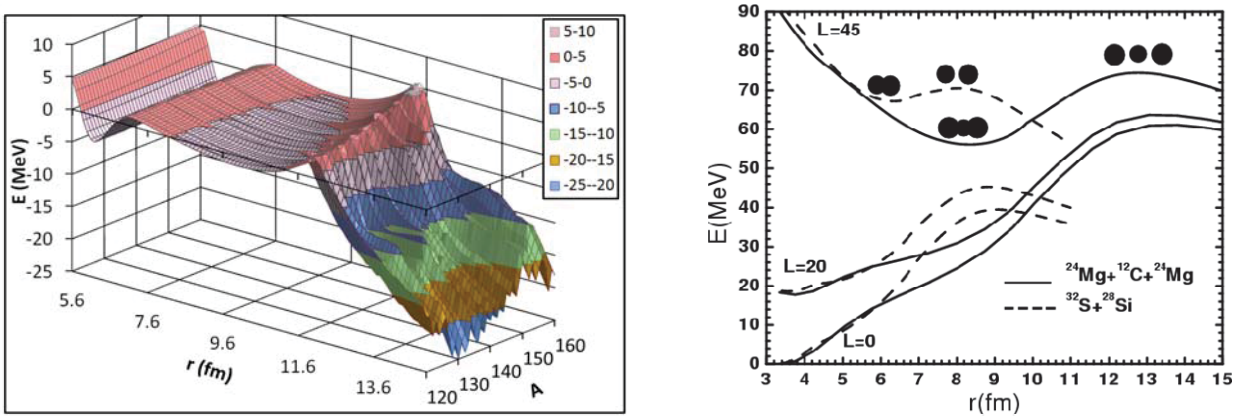

Fig. 5. Multiple-humped macro-microscopic barriers for ^{240}Pu as a function of the heaviest fragment mass (on the *left*) and binary and ternary fission barriers for ^{60}Zn as a function of the angular momentum (on the right).

In the experiments ^{32}S + ^{24}Mg → ^{56}Ni (E*= 84 MeV) and ^{36}Ar + ^{24}Mg → ^{60}Zn (E*= 88 MeV) narrow out-of-plane correlations corresponding to coplanar decay are observed when two fragments are emitted with missing charges from 4 up to 8. This ternary fission have been interpreted as the decay of hyper-deformed states with angular momenta around 45 - 50 $\hbar$ [8].

The Fig. 5 (*right part*) indicates that the very asymmetric ternary fission is favoured relatively to the symmetric ternary one. At high angular momenta around 45 $\hbar$ the potential energy minima is lower in the ternary fission path than in the binary fission path. The more negative Q-value for ternary fission is compensated for the smaller value of the rotational energy at the saddle point. Thus, the GLDM indicates simply that the ternary cluster fission of light nuclei becomes competitive with binary cluster fission at the highest angular momenta.

5. Alpha and Cluster radioactivity

α decay and cluster radioactivity are, as the spontaneous fission, quantum tunneling processes through the potential barrier leading from the mother nucleus to the two emitted fragments. An open question is whether these three decay

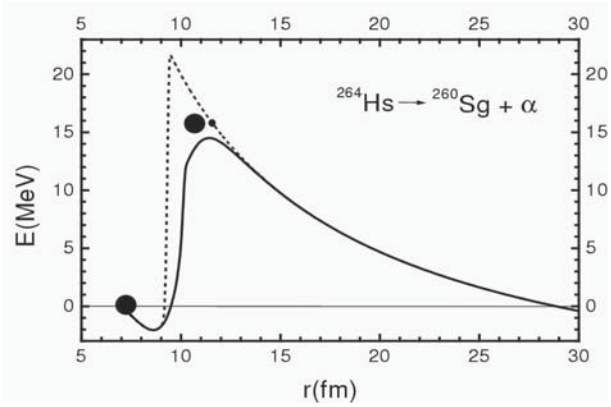

Fig. 6. Potential barriers against alpha emission for the ^{264}Hs nucleus. The dashed curve corresponds to the pure Coulomb barrier without including the proximity energy while the solid line takes into account the proximity effects.

modes can be described within a fission process but for three very different mass asymmetries or whether α and cluster radioactivities correspond to the emission of preformed clusters.

The same GLDM and quasi-molecular shapes has been used [9, 10] to determine the potential barriers for these two decay modes since it is unlikely that the α and cluster emissions lead to elongated fragments contracting after separation. An α decay barrier is displayed in Fig. 6. The difference between the experimental Q value and the theoretical GLDM Q value has been added at the macroscopic energy of the mother nucleus with a linear attenuation factor vanishing at the contact point of the nascent fragments. The proximity forces lower the barriers of 7.3 MeV and the displacement of the maximum is of 2.1 fm.

In the picture of an unified fission model the decay constant has been simply defined as the product of the assault frequency by the barrier penetrability calculated within the WKB method. The main part of the potential barriers corresponding to two-body shapes it has been assumed that the entrance of the tunnel corresponds to the contact point while the inertia parameter is simply the reduced mass. For the cluster emission, these approximations are not possible and the position of the tunnel entrance is the initial sphere while a more sophisticated expression has been selected for the inertia [10, 11]. The Fig. 7 and the Table 2 indicate that this approach allows to determine accurately the half-lives of the α decay and cluster radioactivity. Simple accurate analytical formulas depending on the mass and charge of the α emitter and the experimental or theoretical Q value have been proposed [9] to reproduce the known α decay half-lives and also to predict the half-lives of other possible but still unknown α decays particularly for the superheavy nuclei. Predictions for other cluster emissions have been also provided meeting two criteria: partial half-life $\leq 10^{30}$ s and branching ratio relative to α emission $\geq 10^{-24}$.

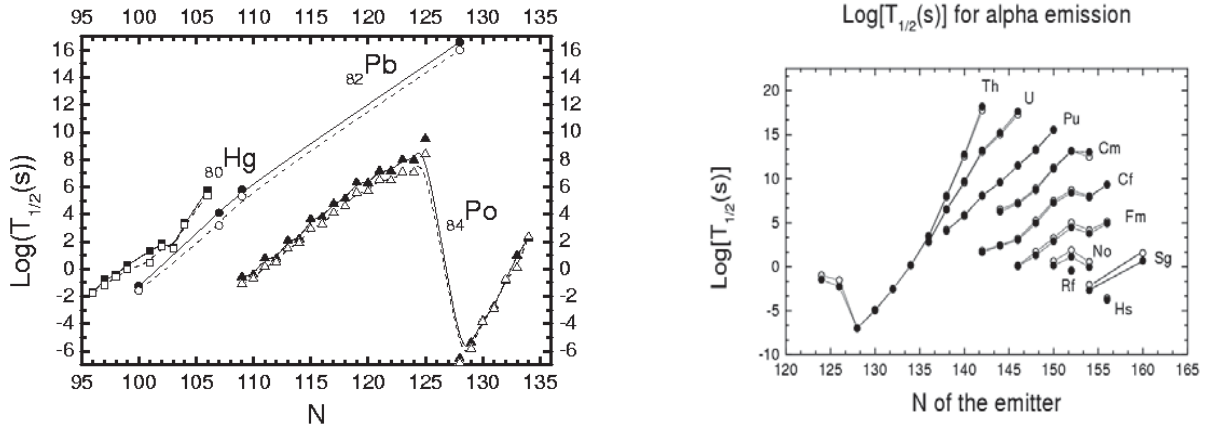

Fig. 7. Comparison between the theoretical and experimental alpha-decay half-lives of the Hg, Pb, Po, Th, U, Pu, Cm, Cf, Fm, No, Rf, Sg and Hs isotopes.

The preformation of clusters and α particle in heavy nuclei has also been investigated [12]. Recently the angular momentum dependence of the partial α decay half-lives has been taken into account and new formulas are proposed.

Table 2. **Comparison between the experimental and theoretical half-lives for the cluster radioactivity**

Emitter and fragments	GLDM-$T_{1/2}$(s)	Experimental $T_{1/2}$(s)
^{222}Ra → ^{14}C + ^{208}Pb	$3.9 \cdot 10^{10}$	$1.0 \cdot 10^{11}$
^{223}Ra → ^{14}C + ^{209}Pb	$2.8 \cdot 10^{13}$	$1.4 \cdot 10^{15}$
^{224}Ra → ^{14}C + ^{210}Pb	$3.9 \cdot 10^{16}$	$5.9 \cdot 10^{15}$
^{226}Ra → ^{14}C + ^{212}Pb	$3.2 \cdot 10^{22}$	$1.8 \cdot 10^{21}$
^{228}Th → ^{20}O + ^{208}Pb	$4.1 \cdot 10^{21}$	$5.0 \cdot 10^{20}$
^{230}Th → ^{24}Ne + ^{206}Hg	$2.8 \cdot 10^{25}$	$4.1 \cdot 10^{24}$
^{231}Pa → ^{24}Ne + ^{207}Tl	$8.6 \cdot 10^{21}$	$7.9 \cdot 10^{22}$
^{232}U → ^{24}Ne + ^{208}Pb	$9.7 \cdot 10^{19}$	$2.5 \cdot 10^{20}$

Continuation of Table 2

Emitter and fragments	GLDM-$T_{1/2}$(s)	Experimental $T_{1/2}$(s)
$^{233}U \rightarrow {}^{24}Ne + {}^{209}Pb$	$2.3 \cdot 10^{23}$	$6.8 \cdot 10^{24}$
$^{234}U \rightarrow {}^{24}Ne + {}^{210}Pb$	$3.5 \cdot 10^{26}$	$7.9 \cdot 10^{25}$
$^{235}U \rightarrow {}^{28}Mg + {}^{207}Hg$	$1.8 \cdot 10^{29}$	$2.8 \cdot 10^{28}$
$^{236}Pu \rightarrow {}^{28}Mg + {}^{208}Pb$	$1.0 \cdot 10^{20}$	$4.7 \cdot 10^{21}$
$^{238}Pu \rightarrow {}^{28}Mg + {}^{210}Pb$	$2.2 \cdot 10^{26}$	$4.7 \cdot 10^{25}$
$^{238}Pu \rightarrow {}^{32}Si + {}^{206}Hg$	$5.4 \cdot 10^{25}$	$1.9 \cdot 10^{25}$

6. Superheavy elements

Using heavy-ion reactions of mean asymmetry (Cr, Fe, Ni, Zn on Bi and Fe, Ni, Zn on Pb) and more recently highly asymmetric reactions (Ca on Np, Pu, Am, Cm, Bk, Cf) new very heavy elements have been synthesized. Actually it is assumed that the lower limit for the fission barrier heights of these heaviest elements is around 6 MeV. The main observed decay mode is the α decay.

Within this GLDM the potential barriers governing these reactions have been determined (see [13] and Fig. 8). For the cold fusion reactions a wide potential pocket due mainly to a high proximity energy and high Coulomb repulsion appears at large deformations. Whatever the microscopic correction assumptions are, double-humped barriers exist. The quasispherical system can be reached by tunnelling even if the shells and pairs are not completely built. Incomplete fusion and fast fission events in the external pocket are the main exit channels since the neck between the two nuclei is formed and exchanges of nucleons can occur. If the reorganization of the single particle levels is very rapid then the value of the proton magic number begins to play some role. So an open question is whether at large deformations the nucleons shells can take form to stabilize the nuclear system before investigating a peculiar exit channel. The pre or post equilibrium nature of the neutron evaporation process is also crucial.

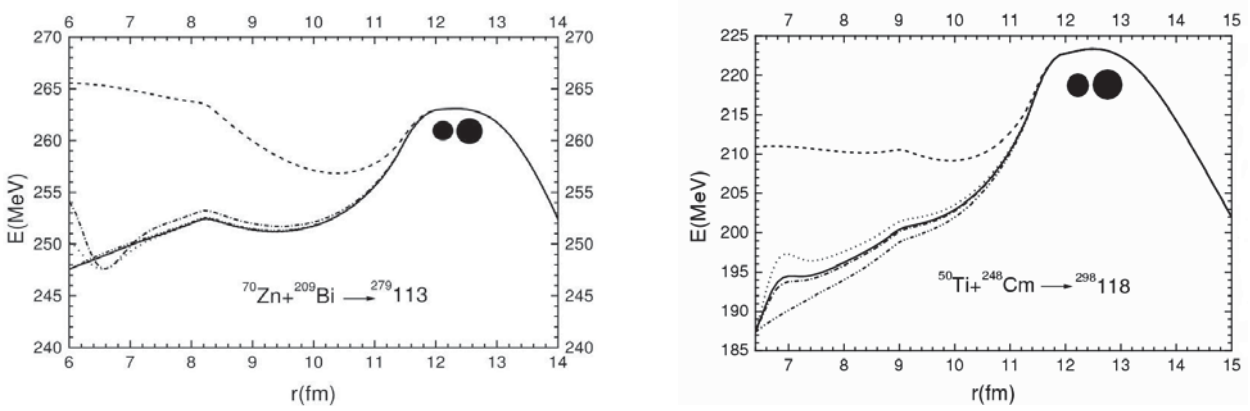

Fig. 8. Potential barriers for the cold $^{70}Zn + {}^{209}Bi$ fusion reaction and the warm $^{50}Ti + {}^{248}Cm$ fusion reaction. The dashed curve corresponds to the macroscopic barrier. The full line, dotted curve and dashed and dotted curve include the shell effects assuming a proton magic number of 114, 120 and 126 and an adjustment to reproduce the Q value.

For the warm fusion reactions the Coulomb repulsion and the proximity energy are lower than for the cold fusion reactions and the barrier against reseparation is wide and high. There is no double-humped barriers. Even for a subbarrier tunnelling of 6 MeV in the entrance channel and even if the shells and pairs have not enough time to develop the nuclear system has enough energy to reach a quasispherical compound system. The excitation energy is more than 30 MeV allowing the emission of several neutrons or an α particle. The different hypotheses on the proton magic number do not change the global predictions in the entrance path.

Using the above mentioned general formulas giving the α decay half-lives and with the help of an accurate Q value our theoretical half-lives agree with the experimental data for the known superheavy nuclei. Thus, predictions of the α decay half-lives of other possible superheavy isotopes have been provided, some of which reaching more than one hour [14].

Recently, the systems ^{238}U + Ni and ^{238}U + Ge have been studied at high excitation energy of 6.62 MeV/u and 6.09 MeV/u possibly leading to nuclear systems of charge 120 and 124 [15]. A coupled analysis of the nuclear reaction time distributions and of the measured K x rays provides evidence for nuclei with Z = 120 and 124 living longer than 10^{-18} s and arising from highly excited compound nuclei.

In Fig. 9 the capture barriers for these reactions have been calculated as a function of the angular momentum within this GLDM. The excitation energy is very large and very high angular momenta are populated while the shell effects are probably very small at these energies. For these very heavy systems the potential energy profile is very flat once the external barrier is passed allowing the possible formation and stability of rapidly rotating isomeric states without necessarily reaching a quasi-spherical nuclear shape and even though the shell effects vanish and the inner barrier is destroyed.

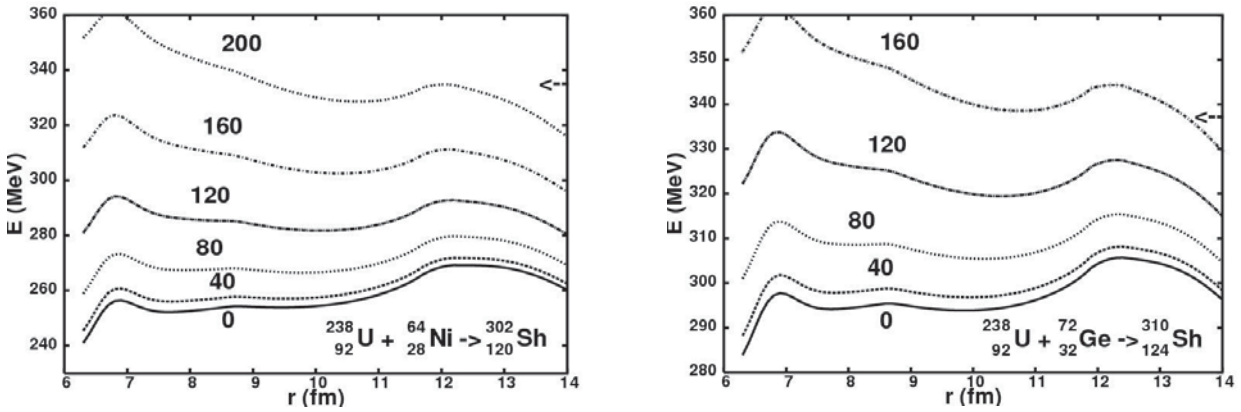

Fig. 9. L-dependent capture barriers for the U + Ni and U + Ge reactions. The arrows indicate the beam energy. The shell effects are taken into account assuming that the next proton magic number is Z = 114.

7. Summary and Conclusions

A generalized liquid drop model including both the mass and charge asymmetries, the proximity energy, a particular nuclear radius, the rotational energy, the shell and pairing energies and the temperature has been defined and used to describe smoothly the transition between two-body and one-body shapes in entrance and exit channels of nuclear reactions.

In the compact and creviced shape valley where the proximity energy is maximal at the contact point, the calculated l-dependent fusion and fission barrier heights and the half-lives of alpha and cluster radioactivities as well as actinides are in agreement with the available experimental data. In this quasi-molecular shape path, double-humped potential barriers begin to appear even macroscopically for heavy nuclear systems in entrance and exit channels due to the influence of the proximity forces and, consequently, quasi-molecular isomeric states can survive in the second minimum of the potential barriers, particularly at intermediate angular momenta.

ACKNOWLEDGMENTS

I thank warmly my colleagues C. Beck, C. Bonilla, V. Yu Denisov, R. Gherghescu, R. K. Gupta, F. Haddad, W. von Oertzen, A. Onillon and H. F. Zhang.

REFERENCES

1. *Royer G., Remaud B.* Static and dynamic fusion barriers in heavy-ion reactions // Nucl. Phys. - 1985. - Vol. A444. - P. 477 - 497.
2. *Krappe H.J., Nix J.R., Sierk A.J.* Unified nuclear potential for heavy-ion elastic scattering, fusion, fission, and ground states masses and deformations // Phys. Rev. - 1979. - Vol. C20. - P. 992 - 1013.
3. *Myers W.D., Swiatecki W.J.* Nuclear properties according to the Thomas - Fermi model // Nucl. Phys. - 1996. - Vol. A601. - P. 141 - 167.
4. *Royer G., Guilbaud M., Onillon A.* Macro-microscopic mass formulae and nuclear mass predictions // Nucl. Phys. - 2010. - Vol. A847. - P. 24 - 41.
5. *Royer G., Remaud B.* Fission processes through compact and creviced shapes // J. Phys. - 1984. - Vol. G10. - P. 1057 - 1070.
6. *Royer G., Gaudillot J.* Rotating hyperdeformed states in light nuclear systems // Phys. Rev. - 2011. - Vol. C84. - P. 044602(6).
7. *Royer G.* Heavy elements and related new phenomena // Fission through quasi-molecular shapes and fragmentation / Ed. by R. K. Gupta, W. Greiner. - Singapure: World Scientific, 1999. - P. 591 - 631.
8. *Von Oertzen W. et al.* Fission decay of N = Z nuclei at high angular momentum: ^{60}Zn // Phys. Rev. - 2008. - Vol. C78. - P. 044615(19).
9. *Royer G.* Alpha emission and spontaneous fission through quasi-molecular shapes // J. Phys. - 2000. - Vol. G26. - P. 1149 - 1170.
10. *Royer G., Gupta R.K., Denisov V.Yu.* Cluster radioactivity and very asymmetric fission through compact and creviced shapes // Nucl. Phys. - 1998. - Vol. A632. - P. 275 - 284.
11. *Bao X.J. et al.* Half-lives of cluster radioactivity with a generalized liquid-drop model // J. Phys. - 2012. - Vol. G39. - P. 095103(11).
12. *Zhang H.F. et al.* Preformation of clusters in heavy nuclei and cluster radioactivity // Phys. Rev. - 2009. - Vol. C80. - P. 037307(4).
13. *Royer G., Zbiri K., Bonilla C.* Entrance channels and alpha decay half-lives of the heaviest elements // Nucl. Phys. - 2004. - Vol. A730. - P. 355 - 376.
14. *Royer G., Zhang H. F.* Recent alpha decay half-lives and analytic expression predictions including the heaviest nuclei // Phys. Rev. - 2008. - Vol. C77. - P. 037602(4).
15. *Frégeau M. O. et al.* X-Ray fluorescence from the element with atomic number Z = 120 // Phys. Rev. Lett. - 2012. - Vol. 108. - P. 122701(5).